A Novel Density Functional Study of the Ground State Properties of a Localized Trinuclear Copper(II,II,III) Mixed-Valence System

Claude Daul,* Sergio Fernandez-Ceballos, Ilaria Ciofini, Cedrick Rauzy, and Carl-Wilhelm Schläpfer[a]

Abstract: Herein we report the analysis of a mixed-valence localized trinuclear copper(II,II,III) cluster by density functional theory. We focused on two peculiar aspects of this system. First we investigated the triplet ground state potential energy surface on a model system. To this end we computed, on the $[E \otimes e]$ adiabatic potential energy surface, the potential energy profile along the *e* mode and constructed ab initio the full potential energy surface (the so called *Mexican hat*), by a fitting procedure. Next, we analyzed the magneto-optical properties of the minimum energy structures. In particular, we applied the single determinant method to compute the full manifold of states arising from the highest occupied molecular orbitals (*magnetic orbitals*). This procedure yielded results in agreement with previous calculations and with the available experimental data when using a model closer to the X-ray structure or when directly dealing with the complete structure of the system.

Keywords: density functional calculations · Jahn–Teller distortion · magnetic properties · mixed-valent compounds ·

Introduction

Mixed-valence systems are polynuclear metal complexes that formally contain metals in different oxidation states. By using the historical classification of Robin and Day,[1] they can be sorted into three classes that are dependent on the degree of localization of the electrons between the different metallic sites. Apart from very well known synthetic examples of mixed-valence systems (such as the Creutz–Taube ion),[2] nature extensively uses these kind of systems whenever electron-transfer reactions (such as in ferridoxins)[3] or oxo-reductive reactions are carried out in biological systems. Many mixed-valence systems form the active sites of metalloproteins or enzymes.

One of the main aims of biochemical synthetic research is to understand, mimic, and reproduce the selectivity and complexity of reactions carried out in nature. Biomimetic compounds, that is compounds that have a topology and a reactivity similar to the natural ones, are interesting owing to the possibility of studying within these *simplified* systems the reactions that normally take place in more complex environments.

[a] Prof. Dr. C. Daul, S. Fernandez-Ceballos, Dr. I. Ciofini, C. Rauzy, Prof. Dr. C.-W. Schläpfer
Department of Chemistry, University of Fribourg
1700 Fribourg (Switzerland)
Fax: +41 26 300 9738
E-mail: claude.daul@unifr.ch

Recently, Cole et al.[4] synthesized and characterized a trinuclear mixed-valence copper complex, $[Cu_3O_2L_3]^{3+}$ L = *N*-permethylated (1*R*,2*R*)-cyclohexanediamine (Figure 1), which

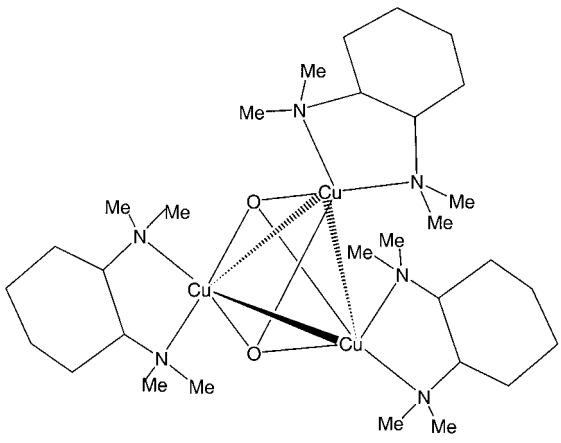

Figure 1. Schematic structure of $[Cu_3O_2L_3]^{3+}$, L = *N*-permethylated (1*R*,2*R*)-cyclohexanediamine (**2**).

exhibits O_2 bond scission as well as reduction of O_2. This compound is particularly interesting because it is the first metal–O_2 complex that leads to full reduction of O_2 in one step with a 3:1 metal:O_2 stoichiometry. In fact, the selective reduction of O_2 by one, two, or four electrons[5–8] is known to happen in the presence of enzymes that contain a copper

 © 2002 WILEY-VCH Verlag GmbH & Co. KGaA, Weinheim 0947-6539/02/0819-4392 $ 20.00+.50/0

active site. Generally, each of the Cu^{I} centers supplies only one electron, therefore one-, two-, or four-electron reductions of O_2 have a 1:2, 1:3, or 1:4 (O_2:metal) stoichiometry, respectively.[9–11] A large variety of enzymes (such as H_2O–lactase, ceruloplasmin, or ascorbate oxidase)[12–16] responsible for four-electron reductions contain a trinuclear Cu active site and a "blue" copper atom at ≈ 12 Å.[13] On the other hand the reduction of O_2 to peroxide is performed in the presence of binuclear Cu active sites (such as in hemocyanin and tyrosinase).[13–17] In the case of the complex discovered by Cole et al.[4] the four electrons are supplied by three copper ions, which leads to a copper(I,II,III) localized system.

From all the available experimental data[4, 18] as well as from subsequent calculations,[18, 19] it has been possible to determine the electronic ground state of this system. X-ray structure analysis data, UV/Vis spectra, NMR susceptibility data, SQUID and MCD data are all consistent with a description of a polynuclear complex, built up from two paramagnetic ($S = 1/2$) Cu^{II} centers, ferromagnetically coupled to give an $S = 1$ ground state, and one diamagnetic (d^8) Cu^{III} center. A previous study[18] has shown that the combination of a large Jahn–Teller distortion and weak electronic coupling is the driving force for the localization of the electrons, while the work of Berces provided a detailed investigation of the thermochemistry of the self-assembly process and the effect of solvation.[19]

Herein we focus on two aspects of the system: its ground state potential energy surface and its magnetic properties, that is the spin manifold at the minimum energy geometry. First we explored the ground state $S = 1$ potential energy surface at a DFT level of a reduced model system along the normal mode responsible for the localization and, by employing a fitting procedure, we extracted the three Jahn–Teller parameters that fully define the $[E \otimes e]$ vibronic coupling problem and the vibrational frequency associated with this localization. Next, both on the minimum energy structure for the model system $[Cu_3O_2(NH_3)_6]^{3+}$ (**1**) and of the full $[Cu_3O_2L_3]^{3+}$ (**2**), optimized at a QM/MM level, we computed the full spin manifold, at a full QM level. The paper is organized as follows: after the explanation the technical details, the results of the computations for the $S = 1$ ground state of the model systems are reported and discussed. Subsequently, the UV/Vis spectra and the singlet–triplet manifold computed for the localized model structure are reported. These latter results are compared both to the available experimental data, to the results of previous calculations[18] based on a different computational method.[20] Finally, the structural parameters and the spin manifold computed for the complete structure of the system **2** are reported and discussed. In this case, the structural optimization was performed at a QM/MM level, while the spin manifold was computed at a full QM (DFT) level.

Computational Methods

All open-shell calculations were performed in a spin-unrestricted formalism. All the calculations on the model system **1** have been performed by using the Amsterdam density functional (ADF) program package.[21] Both the local density approximation (LDA) and the generalized gradient approximation (GGA) for exchange-correlation functionals were used. The LDA was applied with the Xα functional for exchange ($\alpha = 0.7$)[22] and the Vosko, Wilk, and Nusair functional for correlation.[23] The GGA was applied by using the Becke88[24] exchange and the Perdew86[25] correlation (BP), and the Perdew–Wang91[26] (PW91) exchange-correlation functionals. Several calculations were performed including scalar relativistic corrections (Pauli relativistic) as implemented in the ADF.[27] The frozen-core approximation for the inner core electrons was used for all non-hydrogen atoms. The orbitals up to 3p for Cu and 1s for N and O were kept frozen. The valence shells of H, N, and O were described by a double-ζ STO set plus one polarization function. In the case of Cu atoms, a valence triple-ζ plus one polarization function STO basis was used.

Geometry optimizations were performed by using the Broyden–Fletcher–Goldfarb–Shanno algorithm to update the Hessian matrix.[28] The energy convergence criteria for ADF99 used was 10^{-6} au and the default numerical integration was increased (accint = 8.0). If not otherwise specified the calculations were performed for the model system **1**, in which each of the ligands L of $[Cu_3O_2(L_3)]^{3+}$ (L = *N*-permethylated(1*R*,2*R*)-cyclohexanediamine) was substituted by two NH_3 molecules. A schematic representation of the model system **1** and of the reference systems used for D_{3h} and for C_{2v} calculations is given in Figure 2. This modeling, although preserving the donor properties of the ligand L, eliminates the chiral centers. Although commonly performed, this kind of modeling can influence the absolute value of the singlet–triplet splitting significantly.[29] To check this point, supplementary structural optimizations were performed for the real system $[Cu_3O_2(L_3)]^{3+}$ (**2**) at the QM/MM level.

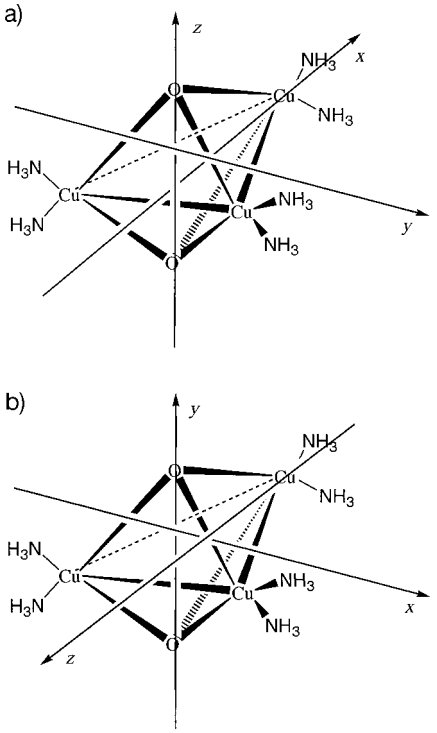

Figure 2. Schematic view of the model system $[Cu_3O_2(NH_3)_6]^{3+}$ (**1**). The reference system used in the calculations in D_{3h} and C_{2v} symmetry are depicted in a) and b) respectively.

The calculations were performed by using the QM/MM implementation in ADF2000.02[30, 31] with the basis set previously described for **1** for the QM part. The QM core was constituted by the $[Cu_3O_2N_6]$ moiety where the link bonds have been capped by hydrogen atoms. The Becke88[24] exchange and the Perdew86[26] correlation (BP) functionals were used for the QM part. The MM part was modeled by using the AMBER force field parameters provided with the program package, and then adding the missing van der Waals parameters for Cu, which were set to values of $E_{min} = 0.0500$, $E_{max} = 12000$, and $\gamma = 12$. Geometry optimization of **2** was performed in C_2

symmetry. Supplementary single-point calculations on the QM/MM optimized structures were performed at the full QM (BP) level. To reach accurate convergence the threshold for ignoring fit integrals (epsfit parameter) was set to 10^{-6} (default value 10^{-4}).

Results and Discussion

Model system: delocalized symmetric structure

The X-ray structure of $[Cu_3O_2L_3]^{3+}$ shows two crystallographically nonequivalent clusters in the unit cell, each of which contains two equivalent and one nonequivalent copper sites.[4] The cores of the two crystallographic units are relatively similar (rms = 0.093 Å). The largest difference is found for the O–O bond length (2.37 versus 2.26 Å). Hereafter we compare the experimental geometry of both of the two crystallographically independent moieties (labeled as Exp.[a] and Exp.[b]) with the results of the calculations. In each moiety, the nonequivalent copper center has very short Cu–O and Cu–N bond lengths (1.83/1.84 and 1.95/1.97 Å, respectively) in agreement with the distances observed for a highly oxidized Cu^{III} complex. The O–O bond is almost cleaved (2.26/2.37 Å), while a typical pseudo-square-planar coordination is found for copper atoms that are coordinated to two nitrogen amine atoms and to the μ_3-oxo bridge.

Geometry optimizations of the model compound **1** were performed for the $S=1$ state in D_{3h} symmetry at different levels of theory. The D_{3h} symmetry is the highest possible for the model system: in this case all three copper centers are symmetry-equivalent. This corresponds to a fully delocalized mixed-valence system. The main geometrical parameters obtained are given in Table 1 and compared to the X-ray data.[4] Regardless of the functional used, the Cu–Cu distance is overestimated (by up to 0.15 Å) even when relativistic effects are included. On the other hand, the Cu–O and the Cu–N bonds are very similar to the average experimental values. Regarding the Cu coordination sphere, the O-Cu-O angle is always underestimated and, as a consequence, the O–O bond length is underestimated by about 0.1 Å if we consider the crystallographic moieties with longer O–O length. On the other hand, the N-Cu-N angle is systematically overestimated. This error is most probably due to the modeling performed. In fact, while in the real system the two amines are held together through a rigid bridge, in the model the two ammonia molecules are let free to relax and the steric repulsion leads to a larger N-Cu-N angle. Subsequent QM/MM calculations where the ligands were explicitly taken into account allowed us to further validate this point (see below).

Looking at the MO energy diagram (Figure 3) and at the plot of the highest occupied MOs $8e_1'$, $5a_2''$, and $6a_2''$ (Figure 4), we notice that they show mainly a d metal and a p O character. However, a significant contribution of the σ donor NH_3 orbital is present. As expected, and in agreement with the results of previous studies,[18, 19] the highest occupied MOs ($6a_2''$ and $7e_1''$) correspond to the linear combination of the highest occupied orbitals on each $CuO_2(NH_3)_2$ moiety, and therefore they show mainly a $d_{x'^2-y'^2}$ metal character (the local coordinate systems on each square-planar moiety pointing towards the ligand are denoted by x' and y'). Qualitatively, we can rationalize the complex as a linear combination of three square-planar subunits carrying one electron for each of the two Cu^{II} centers and no electrons in the highest corresponding $d_{x'^2-y'^2}$ MO in the case of the Cu^{III} center. The symmetry adapted linear combination of these three orbitals leads to the following three frontier MOs in the MO diagram of $[Cu_3O_2(NH_3)_6]^{3+}$: $6a_2''$ and $7e_1''$. The large gap between these three orbitals and the doubly occupied ones deduced from the three d_{z^2} splitting is related to the strong ligand field due to the square-planar environment, which strongly destabilizes the $d_{x'^2-y'^2}$ orbital (pointing towards the ligands) with respect to the other d orbitals. The first unoccupied orbital ($8a_1'$) lies very high in energy (≈4eV above the SOMO; not shown in Figure 3) and it is localized mainly on the NH_3 molecules.

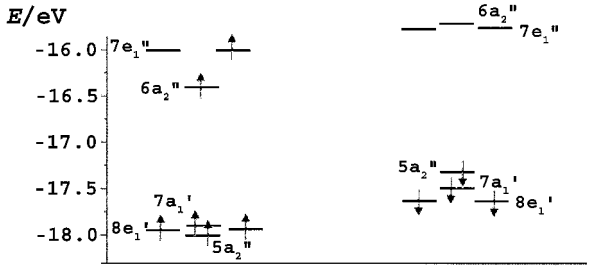

Figure 3. Molecular orbital energy diagram of $[Cu_3O_2(NH_3)_6]^{3+}$ in D_{3h} symmetry.

Owing to the large gap both between the SOMOs and the doubly occupied orbitals as well as between the SOMOs and the LUMO, the active orbitals approximation, that is taking explicitly into account only three orbitals and two electrons, seems to be fully justified for the calculation of the spin manifold. In fact, the energies of excitations originating from the doubly occupied orbital to one of these three orbitals and from the singly occupied orbital to unoccupied orbitals, are high and, therefore, their contributions to the first triplet–singlet gap is negligible.

Table 1. Structural parameters computed for $[Cu_3O_2(NH_3)_6]^{3+}$ in D_{3h}-symmetric structures.[a]

	LDA	BP	PW91	LDA_{rel}	BP_{rel}	$PW91_{rel}$	Exp.[a]	Exp.[b]
d(Cu–Cu)	2.722	2.834	2.824	2.712	2.804	2.795	2.652/2.719	2.641/2.704
d(Cu–O)	1.939	1.991	1.989	1.934	1.981	1.979	1.84/1.94	1.83/2.01
d(Cu–N)	1.998	2.069	2.065	1.996	2.056	2.052	1.97/2.01	1.95/2.04
d(O–O)	2.270	2.270	2.280	2.272	2.285	2.293	2.26	2.37
α(O-Cu-O)	71.7	69.5	69.9	71.9	70.4	70.8	75.8/70.7	72.6(6)/80.4(8)
α(N-Cu-N)	98.6	98.9	98.7	98.4	98.7	98.6	84.5/89.7	84.5/89.7

[a] Rel. = Pauli relativistic. Bond lengths in Å; angles in degrees. Exp.[a] and Exp.[b] see text.

Model system: Jahn–Teller distortion

The Jahn–Teller effect is the intrinsic instability of an electronically degenerate complex towards distortions that remove

© 2002 WILEY-VCH Verlag GmbH & Co. KGaA, Weinheim
0947-6539/02/0819-4394 $ 20.00+.50/0 *Chem. Eur. J.* **2002**, *8*, No. 19

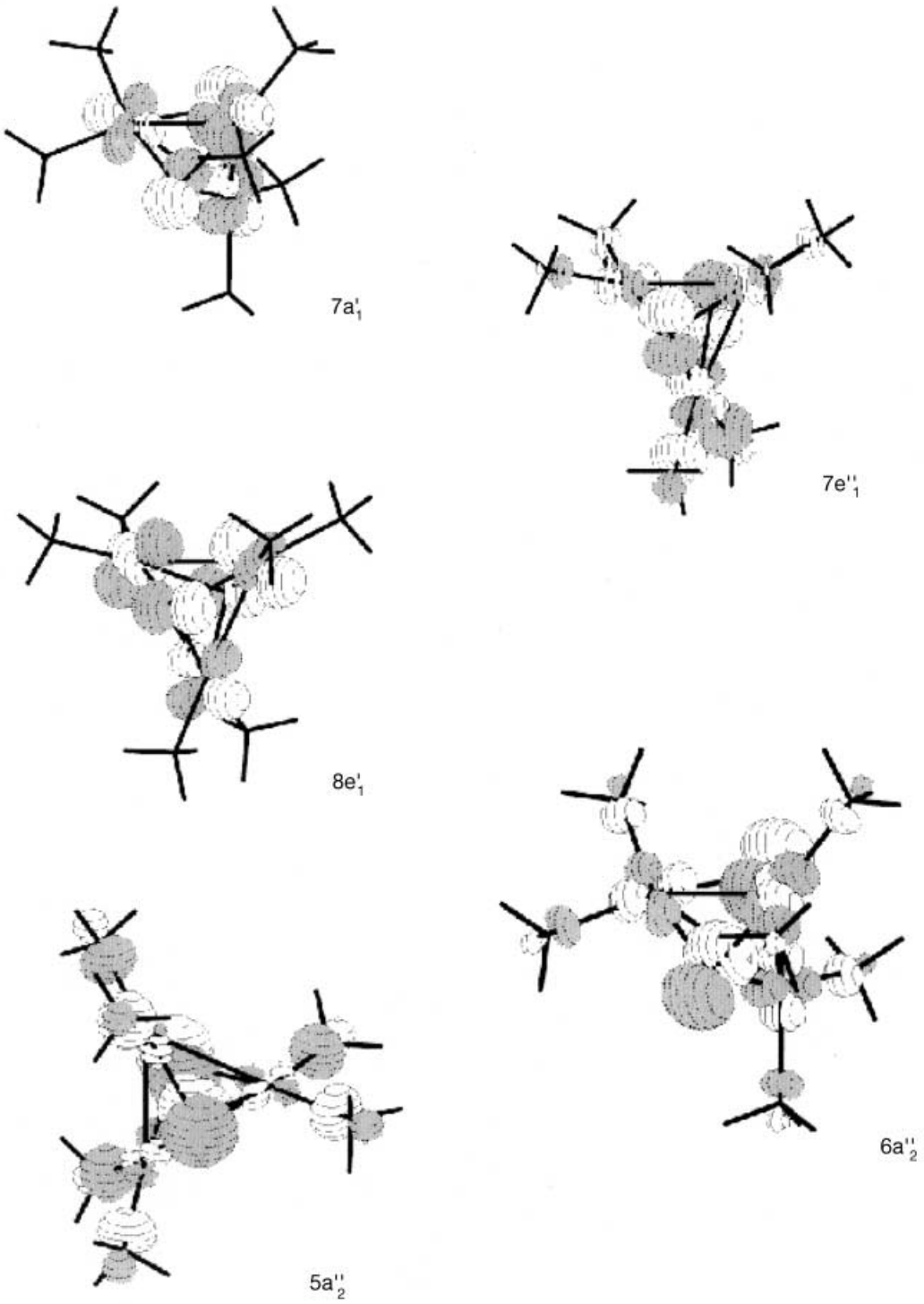

Figure 4. Isovalue representation of the frontier orbitals computed for $[Cu_3O_2(NH_3)_6]^{3+}$ in D_{3h} symmetry. The surfaces have been drawn for $\phi = 0.05(ea_0^{-3})^{1/2}$.

the degeneracy. It was predicted in 1937 by Jahn and Teller[32] but only confirmed experimentally in 1952.[33] Since then Jahn–Teller distortions in transition metal complexes, which is in fact a problem of vibronic interaction, has been studied extensively.[34–39] The D_{3h} MO scheme of $[Cu_3O_2(NH_3)_6]^{3+}$ shows a typical Jahn–Teller active electronic ground state ($^3E_2'$). The consequence of first-order Jahn–Teller interactions is a nuclear displacement which leads to the removal of orbital degeneracy. Therefore, a distortion along the Jahn–Teller active mode has been performed, which leads to a decrease from D_{3h} to C_{2v} symmetry, to fully characterize the system. Although the exact Jahn–Teller mode can be derived by symmetry arguments only in the case of small molecules, the method proposed by Daul et al.[40, 41] has been followed to reproduce the Jahn–Teller–PES as a function of the Jahn–Teller normal mode (Q_{JT}). In this method, the corresponding adiabatic PES can be reconstructed starting from three parameters E_{JT}, Δ, and R_{JT}, or, equivalently, K_E, F_E, and G_E

 © 2002 WILEY-VCH Verlag GmbH & Co. KGaA, Weinheim 0947-6539/02/0819-4395 $ 20.00+.50/0

only. K_E, F_E, and G_E are the force constant and the first- and the second-order vibronic coupling constants, respectively, while E_{JT}, Δ, and R_{JT} are the Jahn–Teller stabilization energy, the minimal barrier height between the minima and the normal coordinate of the Jahn–Teller distorted geometry.

This latter set of parameters can be computed by using the computational procedure explained in reference [40] and summarized for this specific case in Figure 5. The first

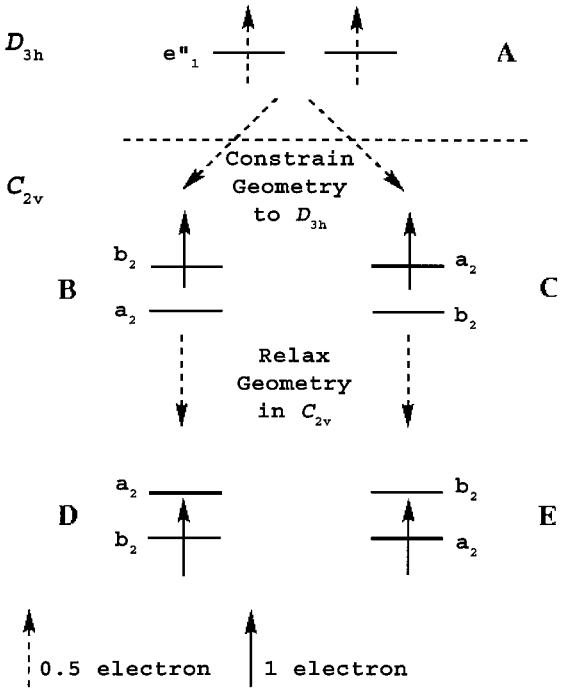

Figure 5. Schematic drawing of the computational method.

calculation (**A**) corresponds to a D_{3h} geometry optimization, while (**B**) and (**C**) are geometry optimizations computed in D_{3h} nuclear symmetry using the C_{2v} electronic symmetry and occupations specified in Figure 5. The lowering of the molecular symmetry from D_{3h} to C_{2v} removes the degeneracy of the e orbitals and leads to a pair of equivalent copper atoms as well as to one nonequivalent copper atom (hereafter Cu_1) as observed in the experimental structure. The three Jahn–Teller parameters, E_{JT}, Δ, and R_{JT}, can be obtained, supposing that **E** has the lowest energy [Expressions (1)–(3)].

$$E_{JT} = E(\mathbf{C}) - E(\mathbf{E}) \quad (1)$$

$$\Delta = [E(\mathbf{C}) - E(\mathbf{E})] - [E(\mathbf{B}) - E(\mathbf{D})] = E(\mathbf{D}) - \mathrm{E}(\mathbf{E}) \quad (2)$$

$$R_{JT} = Q(\mathbf{E}) \quad (3)$$

Generally when using DFT, $E(\mathbf{C}) \neq E(\mathbf{B})$.[41] This problem has been solved by imposing the Expression (2).

R_{JT} was evaluated by using Expression (4), where $\Delta d_i = d_i - d_0$, for which d_i are all the metal-to-ligand distances in the Jahn–Teller distorted geometry and d_0 are the corresponding D_{3h} ones.[42]

$$R_{JT}^2 = \Sigma(\Delta d_i)^2 \quad (4)$$

The optimized geometry corresponding to **E** and to **D** (respectively denoted hereafter as C_{2v2}, $^3B_1$, and C_{2v1}, $^3A_1$) is obtained and is reported in Table 2, and the Jahn—Teller parameters corresponding to the C_{2v2} distortion are reported in Table 3. The experimentally observed static localization is in agreement with the computed Jahn–Teller stabilization energy (E_{JT}; Table 3). The energy difference between the optimized C_{2v} geometries with different occupations (Δ parameter), C_{2v1} and C_{2v2} (E(**D**) and E(**E**), respectively, in Figure 5), is practically negligible: about 10 cm^{-1}. Thus, it cannot be used as a criterion to determine the nature of the localized structure. On the contrary, the corresponding optimized geometries and Mulliken charges are substantially different. In fact, while the C_{2v1} distortion physically corresponds to an expansion of the coordination sphere of the nonequivalent copper atom (Cu_1), the C_{2v2} distortion corresponds to a contraction, which leads to the experimentally observed distortion. The difference of the Cu–O and Cu–N bond lengths computed in D_{3h} symmetry (nuclear and electronic symmetry) and the one computed for the optimized C_{2v1} and C_{2v2} occupations are reported in Table 4. In the case of C_{2v2}, except for the anomalous LDA behavior, we note a significant contraction of the Cu_1–O bonds and the corresponding elongation of the Cu–O (≈ -0.06 Å and $+0.04$ Å, respectively), whereas the Cu–N bonds remain almost unchanged. The distortion to C_{2v2} induces a transfer of charge from the two equivalent copper atoms to the inequivalent copper atom Cu_1, in agreement with a "$1\,Cu^{III} - 2\,Cu^{II}$" description of the system. On the other hand the C_{2v1} distortion yields always to an expansion of the coordination sphere of the non equivalent Cu_1 and a contraction of the one of the equivalent copper atoms.

Finally, we followed the procedure explained in reference [41] to construct the full adiabatic potential energy surface corresponding to the $E \otimes e$ coupling. Therefore, we constructed a series of intermediate geometries between the ones corresponding to **D** and **E** and the ones corresponding to **B** and **C** with the following criterion. Let a be the Cu–Cu distance in D_{3h} symmetry (**B** or **C**), and let b and c be the Cu–Cu distances in C_{2v} (**D** or **E**): three intermediate geometries were constructed by a constrained geometry optimization in which all the geometrical parameters were relaxed except the Cu–Cu distances (b', c') defined according to Expression (5), with $n = 3,2,1$.

$$b' = b + n((a-b)/4)$$
$$c' = c + n((a-c)/4) \quad (5)$$

A least-squares fit of the PES surface computed by using a BP_{rel} approach, following the procedure explained in reference [41], leads to the determination of the three Jahn–Teller parameters, K_E, F_E, and G_E and to the *Mexican hat* plot of Figure 6. In our case the normal mode ($Q\theta$,$Q\varepsilon$) has been simulated by the interpolation between the D_{3h} and C_{2v} geometries, and each of the points has been expressed as mass-weighted coordinates of the structure. The computed K_E, F_E, and G_E values are 421 $cm^{-1}amu^{-2}$, 1368 $cm^{-1}amu^{-1}$, and 1368 $cm^{-1}amu^{-2}$, respectively. Nevertheless, the overall

© 2002 WILEY-VCH Verlag GmbH & Co. KGaA, Weinheim
0947-6539/02/0819-4396 $ 20.00+.50/0 *Chem. Eur. J.* **2002**, *8*, No. 19

Table 2. Structural parameters computed for $[Cu_3O_2(NH_3)_6]^{3+}$ in the two C_{2v} symmetry variations.[a]

	LDA	BP	PW91	LDA_{rel}	BP_{rel}	$PW91_{rel}$	Exp.[a]	Exp.[b]
C_{2v1}								
$d(Cu-Cu_1)$	2.677	2.800	2.791	2.658	2.773	2.765	2.652	2.641
$d(Cu-Cu)$	2.791	2.905	2.896	2.770	2.873	2.866	2.719	2.704
$d(Cu_1-N_1)$	2.018	2.088	2.084	2.006	2.075	2.070	1.972	1.95
$d(Cu_1-O)$	2.005	2.063	2.060	1.999	2.054	2.053	1.839	1.83
$d(Cu-N)$	1.979	2.052	2.047	1.968	2.039	2.035	1.99/2.03	2.01/2.04
$d(Cu-O)$	1.908	1.958	1.956	1.901	1.948	1.94	1.93/1.96	2.01/1.98
$d(O-O)$	2.275	2.261	2.270	2.282	2.277	2.286	2.26	2.37
$d(N_1-N_1)$	3.001	3.098	3.092	2.982	3.752	3.067	2.78	2.73
$d(N-N)$	3.064	3.1724	3.163	3.047	3.151	3.146	2.71	2.86
$\alpha(O\text{-}Cu_1\text{-}O)$	69.1	66.4	66.9	69.6	67.3	67.6	75.8	80.4(8)
$\alpha(Cu\text{-}Cu_1\text{-}Cu)$	62.8	62.8	62.5	62.8	62.4	62.2	61.7	61.7
$\alpha(N_1\text{-}Cu_1\text{-}N_1)$	98.8	98.8	98.7	98.8	98.7	98.9	89.7	88.6
$\alpha(N\text{-}Cu\text{-}N)$	98.5	98.0	98.0	98.5	97.9	97.8	84.5	90.1
$\alpha(O\text{-}Cu\text{-}O)$	73.2	70.5	70.9	73.7	71.5	72.0	70.7	72.6(6)
$\alpha(Cu\text{-}O\text{-}Cu)$	94.0	96.8	95.5	93.5	95.0	94.5	88.3	85.5
$\alpha(Cu\text{-}O\text{-}Cu_1)$	86.3	88.2	88.0	85.9	87.6	87.4	88.3	87.4
dihedral(N-Cu-N-Cu)	146.5	146.0	146.1	146.5	146.0	146.2	138.3	135.7
C_{2v2}								
$d(Cu-Cu_1)$	2.762	2.878	2.866	2.743	2.845	2.837	2.652	2.641
$d(Cu-Cu)$	2.614	2.762	2.752	2.594	2.735	2.727	2.719	2.704
$d(Cu_1-N_1)$	2.975	2.043	2.039	1.964	2.030	2.026	1.972	1.95
$d(Cu_1\text{-}O)$	2.895	1.924	1.923	1.888	1.912	1.913	1.839	1.83
$d(Cu-N)$	2.001	2.074	2.070	1.990	2.062	2.057	1.99/2.03	2.01/2.04
$d(Cu-O)$	1.961	2.028	2.025	1.954	2.020	2.017	1.93/1.96	2.01/1.98
$d(O-O)$	2.277	2.258	2.267	2.283	2.275	2.283	2.26	2.37
$d(N_1-N_1)$	3.017	3.126	3.119	3.006	3.104	3.100	2.78	2.73
$d(N-N)$	3.030	3.117	3.109	3.008	3.092	3.082	2.71	2.86
$\alpha(O\text{-}Cu_1\text{-}O)$	73.8	71.8	72.3	74.4	73.0	73.3	75.8	80.4(8)
$\alpha(Cu\text{-}Cu_1\text{-}Cu)$	56.5	57.3	57.4	56.4	57.4	57.4	61.7	61.7
$\alpha(N_1\text{-}Cu_1\text{-}N_1)$	100.1	99.4	99.3	100.0	99.2	99.0	89.7	88.6
$\alpha(N\text{-}Cu\text{-}N)$	97.8	97.7	97.7	97.8	97.6	97.8	84.5	90.1
$\alpha(O\text{-}Cu\text{-}O)$	70.9	67.6	68.1	71.5	68.5	68.9	70.7	72.6(6)
$\alpha(Cu\text{-}O\text{-}Cu)$	83.6	85.8	85.6	83.2	85.2	85.0	88.3	85.5
$\alpha(Cu\text{-}O\text{-}Cu_1)$	91.5	93.4	93.0	91.1	92.6	92.4	88.3	87.4
dihedral(N-Cu-N-Cu)	138.8	139.0	139.0	138.8	138.9	138.6	138.3	135.7

[a] Rel. = Pauli relativistic. Bond length in Å; angles in degrees. Exp.[a] and Exp.[b] are the structures of the two nonequivalent crystallographic units.

Table 3. Computed Jahn–Teller parameters for the C_{2v2} distortion.[a]

	LDA	BP	PW91	LDA_{rel}	BP_{rel}	$PW91_{rel}$
E_{JT}	0.192	0.185	0.183	0.203	0.188	0.190
Δ	9.54	−8.01	3.84	11.00	−3.94	5.16
R_{JT}	1.93	0.13	0.15	0.11	0.30	0.12

[a] E_{JT} (in eV), Δ (in cm^{-1}), and R_{JT} (in Å). Rel. = Pauli relativistic calculations.

shape of the Mexican hat is invariant under transformation of the coordinate system.

Model system: localized structure

Structural parameters: Hereafter, and in Table 2, Cu_1 denotes the nonequivalent copper atom (formally a Cu^{III}), while the two equivalent copper atoms (formally Cu^{II}) are simply labeled as Cu. As previously discussed the optimized C_{2v} structures for the two different occupations correspond to the two minima along the two orthogonal components of the Jahn–Teller active *e* vibration. While the C_{2v2} occupation yields the observed distortion, one observes for C_{2v1} an expansion for Cu_1 and a contraction for Cu; that is, a breathing of the coordination sphere of the nonequivalent copper atom. If we concentrate on the structural parameters computed for the C_{2v2} occupation, we note a good agreement between the experimental values and the computed ones. Nevertheless, the O–O distance is underestimated, whereas the O-Cu-O angle is well reproduced with respect to the experimental values.

As already pointed out from previous calculations of Root et al.,[18] the O-Cu-O angle, the O–O distance, and the Cu–Cu distance can strongly influence the computed triplet-to-singlet splitting, due to the fact that both the direct and super-exchange pathways are directly influenced by these structural parameters. In particular an elongation of the Cu–Cu bond can lead to a stabilization of the triplet due to a weaker direct interaction, while an increase of the O-Cu-O angle favors a superexchange pathway and it stabilizes the singlet state.

Because of the discrepancy obtained between the optimized and the crystallographic structures, and because of the well-known sensitivity of the spin manifold splitting with respect to structural parameters, we computed the triplet–singlet splitting both for the optimized and for the two crystallographic nonequivalent model structures (vide infra).

As already noted for the fully symmetric D_{3h} structure, the modeling with NH_3 leads to an overestimation of the N–N distance and, as a consequence, of the N-Cu-N angle.

Table 4. Computed difference in bond length (in Å) between: **I**) the optimized D_{3h} geometry (**A**) and the corresponding C_{2v1} ones (**D**); **II**) the optimized D_{3h} geometry (**A**) and the corresponding C_{2v2} ones (**E**). Negative values correspond to a contraction, positive values to an elongation.

	LDA	BP	PW91	LDA_{rel}	BP_{rel}	$PW91_{rel}$
I						
$\Delta(Cu_1-O)$	+0.066	+0.072	+0.071	+0.065	+0.073	+0.074
$\Delta(Cu_1-N_1)$	+0.020	+0.019	+0.019	+0.010	+0.019	+0.018
$\Delta(Cu-O)$	−0.031	−0.033	−0.033	−0.033	−0.033	−0.039
$\Delta(Cu-N)$	−0.019	−0.014	−0.018	−0.028	−0.017	−0.017
II						
$\Delta(Cu_1-O)$	+0.956	−0.067	−0.066	−0.046	−0.069	−0.066
$\Delta(Cu_1-N_1)$	+0.977	−0.026	−0.026	−0.032	−0.026	−0.026
$\Delta(Cu-O)$	0.022	+0.041	+0.036	+0.020	+0.039	+0.036
$\Delta(Cu-N)$	$+3\times10^{-3}$	$+5\times10^{-3}$	$+5\times10^{-3}$	-6×10^{-3}	$+6\times10^{-3}$	$+5\times10^{-3}$

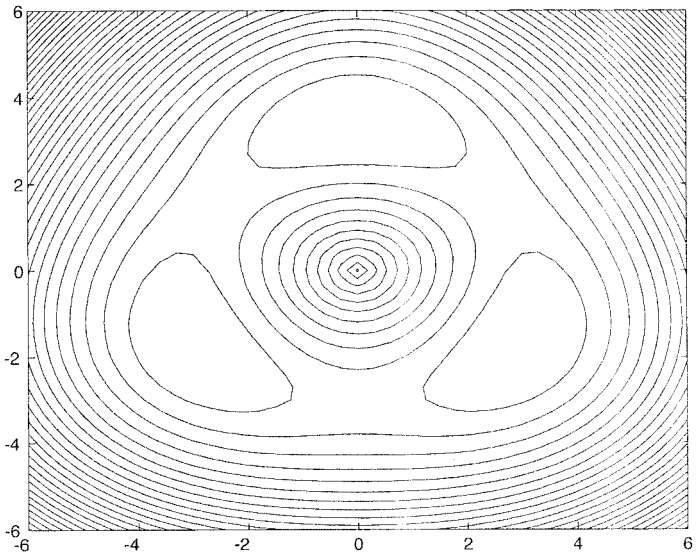

Figure 6. Computed adiabatic PES corresponding to the $E \otimes e$ coupling for $[Cu_3O_2(NH_3)_6]^{3+}$.

Furthermore, as a general trend, although copper is only a 3d metal, significant effects on geometry are noted when relativistic effects are included within the Pauli approximation.

Calculation of UV/Vis spectra: The experimental spectrum of $[Cu_3O_2L_3]^{3+}$, recorded in CH_2Cl_2 at $-80\,^{\circ}C$, shows four main bands at 290 (4.27), 355 (3.49), 480 (2.58), and 620 nm (1.99 eV).[4] The two more intense, high-energy transitions, have been experimentally attributed to ligand-to-metal charge transfer (LMCT), whereas the other two bands are of lower intensity.

The UV/Vis spectrum of the complex of the optimized C_{2v2} geometry has been computed by using the Slater transition state (STS) method.[22] Only symmetry and spin (i.e. triplet–triplet) allowed transitions were computed. In this method only one electron excitation is taken into account and no estimation of the intensity of transitions can be given. The MO energy diagram computed at a LDA_{rel} level, corresponding to a C_{2v2} occupation, is reported in Figure 7.

The first optical transition, in a harmonic approximation, is related to the Jahn–Teller stabilization energy (E_{JT}) following Sturge's development (see Expression (6)).[43]

$$\Delta E \cong 4\,E_{JT} \qquad (6)$$

If we compute $4\,E_{JT}$ from the value for E_{JT} reported in Table 3, we obtain a ΔE value that is less than half of the experimental value of the first transition and is out of the range of UV/Vis spectroscopy. The first optical transition is therefore not attributed to the transition between the split levels stemming from the $^3E''_2$ state but to a transition from the first doubly occupied orbitals to the SOMOs ($d \rightarrow d$ transition).

Looking at the MO diagram in Figure 7, we see that the $11b_2^{\beta} \rightarrow 12b_2^{\beta}$ and the $10_1^{\beta} \rightarrow 12b_2^{\beta}$ one-electron excitations

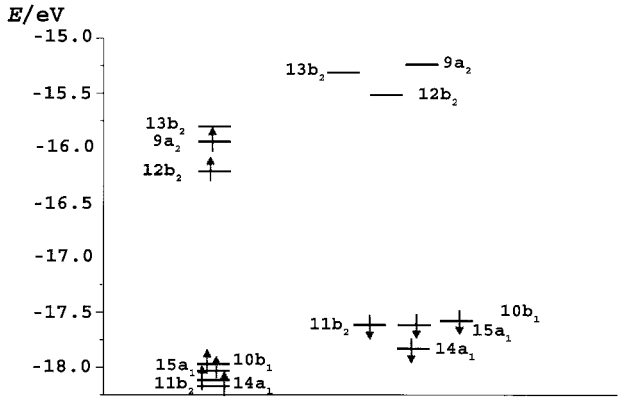

Figure 7. Schematic representation of the nine non-redundant single determinants.

contribute to the first UV/Vis transition, and the $11b_2^{\beta} \rightarrow 9a_2^{\beta}$ to the second UV/Vis transition. The LMCT transitions were identified as $9b_2^{\beta} \rightarrow 12b_2^{\beta}$ and $6a_2^{\beta} \rightarrow 12b_2^{\beta}$. The assignment of the LMCT is straightforward because the O-centered MOs are easy to identify.

The computed electronic transitions are collected in Table 5. Generally, the energy of the transitions is underestimated by using the STS method. An exception is the first LMCT, which is always overestimated. As a matter of fact the STS method does not give very accurate results, but, due to the system size, we could not afford to use more sophisticated techniques. In any case the underestimation of the transition energy is somehow expected due to the lack of full relaxation, which isintrinsic to the method.

Table 5. Computed UV/Vis transition (in eV) of $[Cu_3O_2(NH_3)_6]^{3+}$ in the optimized C_{2v2} geometries.

	LDA_{rel}	$PW91_{rel}$	BP_{rel}	Exp.	Assignment
$11b_2^{\beta} \rightarrow 12b_2^{\beta}$	1.97	1.58	1.70	1.99	d–d
$10b_1^{\beta} \rightarrow 12b_2^{\beta}$	2.05	1.83	1.95	1.99	d–d
$11b_2^{\beta} \rightarrow 9a_2^{\beta}$	2.38	2.02	2.03	2.58	d–d
$9b_2^{\beta} \rightarrow 12b_2^{\beta}$	4.15	3.70	3.79	3.49	LMCT
$6a_2^{\beta} \rightarrow 12b_2^{\beta}$	4.40	3.95	4.14	4.27	LMCT

Magnetic properties: *J*: To compute the low-energy spin states of the complex, the single determinant (SD) method was used.[44] This method exploits the full multideterminant nature of an open-shell state as a linear combination of Slater determinants.[44] This yields first-order expressions for the multiplet energies which are linear combinations of SD energies. To calculate these quantities, both spatial and spin symmetry are fully exploited. This method was first developed for the calculation of optical transitions,[45] and has been recently applied to the calculation of exchange-coupling constants in a number of different systems.[46, 47] Some approximations and limitations in the practical implementation of the method are:

 © 2002 WILEY-VCH Verlag GmbH & Co. KGaA, Weinheim 0947-6539/02/0819-4398 $ 20.00+.50/0 *Chem. Eur. J.* **2002**, *8*, No. 19

- The method does not consider the two-electron second-order terms, which are neither exchange nor Coulomb, and which can, in general, not be expressed in terms of energies of single determinants.
- The method is usually applied within the active electrons approximation. In this case it is possible to include second-order electrostatic interactions precisely. Hence, frequently, only the microstates arising from the different occupations of the active orbitals are taken into account.

Owing to the large splitting between the doubly occupied orbitals and the SOMOs and between the LUMO and the LUMO + 1, only the SOMO and the LUMO were considered as active orbitals, leading to a problem of two electrons in three orbitals.

Referring to the MO scheme of Figure 7, these orbitals belong to the irrep. $12b_2$, $9a_2$, and $13b_2$. From their occupation with two electrons, nine states can be generated: four $^1A_1$, two $^1B_1$, two $^3B_1$, and one $^3A_1$.

Neglecting the electrostatic matrix elements which are neither exchange nor Coulomb, the energy of these spin states can be expressed in terms of the energy of the nine non-redundant single determinants (NRSD) depicted in Figure 8 and Expression (7).

$$
\begin{aligned}
{}^1A_1 &= \begin{bmatrix} E(4) & -E(0)+E(7) & -E(5)+E(6) & 0 \\ -E(0)+E(7) & E(1) & -E(8)+E(3) & 0 \\ -E(5)+E(6) & -E(8)+E(3) & E(2) & 0 \\ 0 & 0 & 0 & -E(8)+2E(3) \end{bmatrix} \\
{}^1B_1 &= \begin{bmatrix} -E(0)+2E(7) & 0 \\ 0 & -E(5)+2E(6) \end{bmatrix} \\
{}^3B_1 &= \begin{bmatrix} E(0) & 0 \\ 0 & E(5) \end{bmatrix} \\
{}^3A_1 &= E(8)
\end{aligned}
\qquad (7)
$$

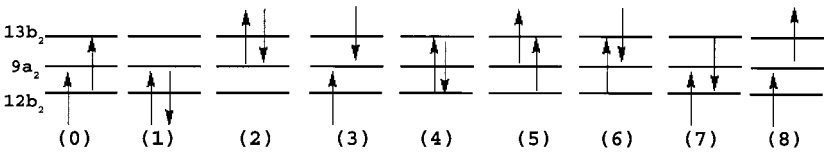

Figure 8. Molecular orbital energy diagram of $[Cu_3O_2(NH_3)_6]^{3+}$ in C_{2v} symmetry using occupation C_{2v2}.

Diagonalization of the $^1A_1$ matrix leads to the energy of the four $^1A_1$ states.

The spin manifold computed both at the LDA and GGA Pauli relativistic level for the corresponding C_{2v2}-optimized structures is reported in Table 6. As expected, the gound state is the $^3B_1$ (C_{2v2} state). The 1^3B_1 to 1^3A_1 splitting corresponds to the transition between the split levels of the $^3E_2''$ state. The computed values are far from to the ones expected by using the harmonic approximation of Sturge et al.[43] and the computed E_{JT} value given in Table 3, being 0.33 eV, 0.98 eV, and 0.36 eV versus 0.81 eV, 0.76 eV, and 0.75 eV for LDA_{rel}, $PW91_{rel}$, and BP_{rel} respectively. This result suggests a strong anharmonicity of the potential energy surface. This is confirmed by the relatively large value of F_E which is the linear vibronic term in the $[E \otimes e]$ coupling.[48]

Table 6. Computed energy of the different spin states at LDA and GGA level relative to the $^3B_1$ ground state energy of $[Cu_3O_2(NH_3)_6]^{3+}$ in the optimized C_{2v2} geometries. Energy in eV.

	LDA_{rel}	$PW91_{rel}$	BP_{rel}
$1\ ^3B_1$	0	0	0
$2\ ^3B_1$	0.4974	0.5148	0.5293
$1\ ^3A_1$	0.3348	0.9848	0.3629
$1\ ^1A_1$	0.2015	0.3710	0.1026
$2\ ^1A_1$	0.8803	0.8509	0.8853
$3\ ^1A_1$	0.5960	2.5405	1.9353
$4\ ^1A_1$	2.7188	2.7046	2.9830
$1\ ^1B_1$	0.6696	0.4559	0.4634
$2\ ^1B_1$	0.8807	0.8077	0.8131

The difference in energy between the triplet ground state and the first singlet state is relatively large (0.20 eV for LDA, 0.10 eV for BP, and 0.37 eV for PW91). Although in agreement with the results of a previous calculation by Root et al.,[18] the computation largely overestimates the experimental gap (14 cm^{-1}). Root et al.[18] attributed this discrepancy to the peculiar method they were using, that is the broken symmetry technique.[20] Unfortunately, this seems not to be the case. In fact, even if the single determinant method takes into account the complete three-orbital-two-electron manifold, and corrections are made for some of the assumptions of the broken symmetry method our results are not significantly better than the ones of Root et al.[18]

To better elucidate this point, we decided to analyze the effect of nuclear geometry on the computed splitting of the spin manifold. For this, we computed the triplet–singlet energy gap (first-order) for the two nonequivalent crystallographic clusters where, as previously, the ligand L was substituted by two NH_3 molecules, and the nitrogen center was maintained at the position it adopts in the crystal structure.

At the LDA level, the computed triplet-to-singlet energy gap is 25 cm^{-1} for the crystallographic units with an O–O distance of 2.26 Å (Exp.[a] in Table 2) and 550 cm^{-1} for the one with an O–O distance of 2.37 Å (Exp.[b] in Table 2).

The agreement with the experimental data is significantly improved, thus confirming the strong effect of structure on the computed magnetic properties.

Complete structure of the system: structural and magnetic properties

To test the influence of the ligand L = *N*-permethylated (1*R*,2*R*)-cyclohexanediamine both on the geometric and electronic structure, we performed supplementary calculations on the complete structure of the system **2**. Structural optimizations were performed at the QM/MM level for the localized structures (symmetry C_2) for the two occupations corresponding to the C_{2v1} and C_{2v2} occupations previously discussed for the model system **1**. In the case of the C_2

 © 2002 WILEY-VCH Verlag GmbH & Co. KGaA, Weinheim 0947-6539/02/0819-4399 $ 20.00+.50/0

calculations, this yields ^3A and ^3B states, respectively. The optimized structures are reported in Table 7, and compared with the corresponding model structures and experimental one.

While a general better agreement of the $^3B_1$ structure with the experimental data can be remarked, actually only small changes of the $Cu_3O_2N_6$ core are apparent. The Cu–O and Cu–N distances are practically unchanged on comparing the model system **1** and the real complexes **2**. This is not surprising since the direct effect of the ligand on the core is presumably small and since the ligand has been considered only at the MM level. Nevertheless one substantial change is clearly evident when the complete structure of the system is compared with the model one: the N-Cu-N angle which was overestimated for the model is now reduced by approximately 10° towards the experimental value. As already emphasized this is due to the fact that in the model no steric constrain was applied to hold the NH_3 molecules together.

Both direct and indirect (geometrical) effects of the modeling on the computed spin manifold can now be evaluated. The triplet–singlet energy gap was computed (with the single determinant techinique) for the QM/MM-optimized structure at a full QM level in the case of the ^3B geometry. The triplet–singlet gap is computed to be 72 cm^{-1} at the BP level; thus, substantially improving the results obtained for the model systems (800 cm^{-1} at the BP_{rel} level). When the complete X-ray structure of the two crystallographic moieties is used, the triplet–singlet gap at a first approximation is computed to be 157 cm^{-1} for Exp.[a] and 340 cm^{-1} for Exp.[b]. From all these results, the following conclusions can be drawn:

- Neglecting the full ligand has mainly structural effects (i.e. the change of the N-Cu-N angle) that indireclty affect the computed spin manifold.
- The direct effect of the ligand on the electronic structure of the core is negligible since the results obtained for model X-ray structures (25 cm^{-1} and 550 cm^{-1}) and the full X-ray structure (157 cm^{-1} and 340 cm^{-1}) are practically equivalent within the error range of the methodology.
- The modeling retains all the electronic features of the system in terms of exchange and super-exchange pathways, but allows a structural flexibility that the complete structure of the system does not possess.

In conclusion, the modeling we performed influences the triplet–singlet energy gap only with respect to structural effects, while from an electronic point of view it reproduces correctly the core of the system. It also worthwhile to recall that discrepancies between the experimental and the computed values are also due in part to the approximations implicit in the methodology we apply and better agreement is not expected if not fortuitous.

Finally, we can conclude that, when dealing with a complex molecular system, a QM/MM approach for structural optimization combined with DFT calculations for the spin manifold yield a quantitative description of the magnetic properties of the system.

Table 7. Structural parameters computed at the BP level for $[Cu_3O_2(NH_3)_6]^{3+}$ in C_{2v} symmetry (**1**) and for $[Cu_3O_2L_3]^{3+}$ in C_2 symmetry (**2**) with different occupations.[a]

	$^3A_1$(**1**)	^3A(**2**)	$^3B_1$(**1**)	^3B(**2**)	Exp.[a]	Exp.[b]
d(Cu–Cu_1)	2.800	2.783	2.878	2.821	2.652	2.641
d(Cu–Cu)	2.905	2.833	2.762	2.783	2.719	2.704
d(Cu_1–N_1)	2.088	2.015	2.043	2.053	1.972	1.95
d(Cu_1–O)	2.063	2.017	1.924	1.903	1.839	1.83
d(Cu–N)	2.052	2.059/2.016	2.074	2.078/2.081	1.99/2.03	2.01/2.04
d(Cu–O)	1.958	1.946/1.936	2.028	2.001/2.006	1.93/1.96	2.01/1.98
d(O–O)	2.261	2.235	2.258	2.232	2.26	2.37
d(N_1–N_1)	3.098	2.856	3.126	2.839	2.78	2.73
d(N–N)	3.172	2.845	3.117	2.858	2.71	2.86
α(O-Cu_1-O)	66.4	67.3	71.8	72.0	75.8	80.4(8)
α(Cu-Cu_1-Cu)	62.5	61.2	57.3	59.1	61.7	61.7
α(N_1-Cu_1-N_1)	98.8	85.9	99.4	87.5	89.7	88.6
α(N-Cu-N)	98.0	87.3	97.7	86.6	84.5	90.1
α(O-Cu-O)	70.5	70.3	67.6	67.7	70.7	72.6(6)
α(Cu-O-Cu)	96.8	93.7	85.8	88.0	88.3	85.5
α(Cu-O-Cu_1)	88.2	89.5	93.4	92.5	88.3	87.4
dihedral(N-Cu-N-Cu)	146.0	139.6	139.0	137.2	138.3	135.7

[a] Bond length in Å; angles in degrees. Exp.[a] and Exp.[b] are the structures of the two nonequivalent crystallographic units.

Conclusion

An analysis of the ground state properties of a trinuclear copper system of biochemical interest has been performed on a model cluster by using density functional theory. The electronic structure of the experimentally observed distorted cluster has been identified and analyzed through a computation of the potential energy surface of the ground state.

A localized system with 2 Cu^{II} and 1 Cu^{III} centers has been found to be more stable than the delocalized structure with three equivalent Cu atoms. For this localized structure, UV/Vis transitions and spin manifold splitting have been computed. From these results two major conclusions can be drawn: First, it has been demonstrated that DFT is a powerful technique for the study of mixed-valence systems; it is capable of reproducing the PES along the localization/delocalization vibrational mode. This is true also in case of localized systems. Second, while calculations based on the truncated structure, neglecting the crystal environment, do not strongly perturb the qualitative shape of the PES, they are of substantial importance whenever a direct comparison between the computed and experimental magnetic properties is sought.

Therefore, QM calculations were performed to test the effect of the ligand both on the structure and on the computed spin manifold. The improved agreement between the experimental data and that computed provides further support for the strong influence small structural changes have on the observed magnetic be-

© 2002 WILEY-VCH Verlag GmbH & Co. KGaA, Weinheim
0947-6539/02/0819-4400 $ 20.00+.50/0 *Chem. Eur. J.* **2002**, *8*, No. 19

havior. This further emphasizes the necessity of correctly treating the complete structure of a system (including solvent or crystal environment) in quantum-chemical calculations.

Acknowledgement

This work was supported by the Swiss National Science Foundation. S.F.-C. acknowledges an Erasmus/Socrates grant.

[1] M. B. Robin, P. Day, H. B. Burgi, *Adv. Inorg. Chem. Radio. Chem.* **1967**, *10*, 247.
[2] C. Creutz, H. Taube, *J. Am. Chem. Soc.* **1969**, *91*, 3988.
[3] O. Kahn, *Molecular Magnetism*, VCH Publisher, **1993**.
[4] A. P. Cole, D. E. Root, P. Mukherjee, E. I. Solomon, T. D. P. Stack, *Science*, **1996**, *273*, 1848.
[5] *Bioinorganic Chemistry of Copper* (Eds.: K. D. Karlin, Z. Tyeklàr), Chapman & Hall, New York, **1993**.
[6] N. Kitajima, Y. Moro-oka, *Chem. Rev.* **1994**, *94*, 737.
[7] a) E. I. Solomon, M. J. Baldwin, M. D. Lowery, *Chem. Rev.* **1992**, *92*, 521; b) E. I. Solomon, M. D. Lowery, *Science*, **1993**, *259*, 1575.
[8] K. D. Karlin, S. Fox, *Active Oxygen in Biochemistry* (Eds.: J. S. Valentine, C. S. Foote, A. Greenberg, J. F. Liebman), Chapman & Hall, Glasgow, **1995**, 188–231.
[9] a) K. Fujisawa, M. Tanaka, Y. Moro-oka, N. J. Kitajima, *J. Am. Chem. Soc.* **1994**, *116*, 12079; b) M. Harata, K. Jitsukawa, H. Masuda, H. J. Einaga, *J. Am. Chem. Soc.* **1994**, *116*, 10817.
[10] K. A. Magnus, H. Ton-That, J. E. Carpenter, *Chem. Rev.* **1994**, *94*, 727.
[11] a) T. N. Sorrel, W. E. Allen, P. S. White, *Inorg. Chem.* **1995**, *34*, 952; b) W. E. Lynch, D. M. Kurtz, S. K. Wang, R. A. J. Scott, *J. Am. Chem. Soc.* **1994**, *116*, 11030; c) S. Mahapatra, J. A. Halfen, E. C. Wilkinson, L. Que, Jr., W. B. Tolman, *J. Am. Chem. Soc.* **1994**, *116*, 9785.
[12] D. J. Spira-Solomon, M. D. Allendorf, E. I. J. Solomon, *J. Am. Chem. Soc.* **1986**, *108*, 5318.
[13] A. J. Messerschmidt, *Mol. Biol.* **1992**, *224*, 179.
[14] a) M. D. Allendorf, D. J. Spira, E. I. Solomon, *Proc. Natl. Acad. Sci. USA* **1985**, *82*, 3063; b) L. Ryden, I. Björk, *Biochemistry* **1976**, *15*, 3411; c) I. Zaitseva, *J. Biol. Inorg. Chem.* **1996**, *1*, 15.
[15] A. Messerschmidt, H. Luecke, R. Huber, *J. Mol. Biol.* **1993**, *230*, 997.
[16] J. L. Cole, P. A. Clark, E. I. J. Solomon, *J. Am. Chem. Soc.* **1990**, *112*, 9534.
[17] J. L. Cole, G. O. Tan, E. K. Yang, K. O. Hodgson, E. I. J. Solomon, *J. Am. Chem. Soc.* **1990**, *112*, 2243.
[18] D. E. Root, M. J. Henson, T. Machonkin, P. Mukherjee, T. D. P. Stack, E. I. Solomon, *J. Am. Chem. Soc.* **1998**, *120*, 4982.
[19] A. Berces, *Chem. Eur. J.* **1998**, *4*, 1297.
[20] a) L. Noodleman, J. G. Norman, Jr., *J. Chem. Phys.* **1979**, *70*, 4903; b) L. J. Noodleman, *Chem. Phys.* **1981**, *74*, 5737.
[21] Amsterdam Density Functional (ADF), **1999**. Scientific Computing and Modelling, Theorectical Chemistry, Vrije Universiteit, Amsterdam, **1997**. a) E. J. Baerends, D. E. Ellis, P. Ros, *Chem. Phys.* **1973**, *2*, 42. b) P. M. Boerrigter, G. Te Velde, E. J. Baerends, *Int. J. Quantum Chem.* **1988**, *33*, 87; c) G. Te velde, E. J. Baerends, *J. Comput. Phys.* **1992**, *99*, 84; d) C. Fonseca Guerra, O. Visser, J. G. Snijders, G. Te Velde, E. J. Baerends in *Methods and Techniques in Computational Chemistry* (Eds.: E. Clementi, C. Corongiu), STEF, Cagliari, **1995**, Chap. 8, p. 305.
[22] J. C. Slater, "Self Consistent Field for Molecules and Solids" in *Quantum Theory of Molecules and Solids*, *Vol. 4*, McGraw-Hill, New York, **1974**.
[23] S. H. Vosko, L. Wilk, M. Nusair, *Can. J. Phys.* **1980**, *58*, 1200.
[24] A. D. Becke, *Phys. Rev. B* **1980**, *38*, 3098.
[25] J. P. Perdew, *Phys. Rev. B* **1986**, *33*, 8822.
[26] J. P. Perdew, J. A. Chevary, S. H. Vosko, K. A. Jackson, M. R. Pederson, D. J. Singh, C. Fiolhais, *Phys. Rev. B* **1992**, *46*, 6671.
[27] J. G. Snijder, E. J. Baerends, *Mol. Phys.* **1978**, *36*, 1789.
[28] W. H. Press, B. P. Flannery, S. A. Teukolsky, W. T. Vetterling, *Numerical Recipes*, Cambridge University Press, Cambridge, **1989**.
[29] C. Adamo, V. Barone, A. Bencini, F. Totti, I. Ciofini, *Inorg. Chem.* **1999**, *38*, 1996.
[30] T. K. Woo, L. Cavallo, T. Ziegler, Theor. Chem. Acc. **1998**, *100*, 307.
[31] F. Maseras, K. Morokuma, *J. Comp. Chem.* **1995**, *16*, 1170.
[32] H. A. Jahn, E. Teller, *Proc. Roy. Soc.* **1937**, *A161*, 220.
[33] B. Bleaney, K. D. Bowers, *Proc. Phys. Soc.* **1952**, *A65*, 667.
[34] I. B. Bersuker, *The Jahn–Teller Effect and Vibronic Interactions in Modern Chemistry*, Plenum Press, London, **1984**.
[35] C. J. Ballhausen, *Molecular Electronic Structures of Transition Metal Complexes*, McGraw-Hill, New York, **1979**.
[36] C. J. Ballhausen, *Vibronic Processes in Inorganic Chemistry*, (Ed.: C. F. Flint), Kluwer, Dordrecht, **1989**, 53–78.
[37] I. B. Bersuker, *Electronic Structure and Properties of Transition Metal Compounds*, Wiley, New York, **1996**, Chapter 7.
[38] I. B. Bersuker, V. Z. Polinger, *Vibronic Interactions in Molecules and Crystals*, Springer, Berlin, **1989**.
[39] *The Dynamical Jahn–Teller Effect in Localized Systems* (Eds.: Yu. E. Perlin, M. Wagner) North-Holland, Amsterdam, **1984**.
[40] T. K. Kundu, R. Bruyndonckx, C. A. Daul, P. T. Manoharan, *Inorg. Chem.* **1999**, *38*, 3931.
[41] R. Bruyndonckx, C. Daul, P. T. Manoharan, E. Deiss. *Inorg. Chem.* **1997**, *36*, 4251–4256.
[42] E. Gamp, "ESR-Untersuchungen über den Jahn-Teller-Effeckt in oktaedrishen Kupfer(II)-Komplexen", PhD Thesis, St. Gallen (Switzerland), **1949**.
[43] M. D. Sturge, *Solid State Phys.* **1968**, *20*, 91.
[44] a) C. Daul, *Int. J. Quant. Chem.* **1994**, *52*, 867; b) T. Ziegler, A. Rauk, E. J. Baerends, *Theor. Chim. Acta* **1977**, *43*, 261; c) C. Daul, E. J. Baerends, P.Vernooijs, *Inorg. Chem.* **1994**, *33*, 3538.
[45] C. A. Daul, K. Doclo, A. C. Stukl in *Recent Advance in Density Functional Methods*, *Part II* (Ed.: D. P. Chong), World Scientific Publischers **1997**, 61.
[46] A. Bencini, F. Totti, C. A. Daul, K. Doclo, P. Fantucci, V. Barone, *Inorg. Chem.* **1997**, *36*, 5022.
[47] A. Bencini, I. Ciofini, E. Giannasi, C. A. Daul, K. Doclo, *Inorg. Chem.* **1998**, *37*, 3719.
[48] I. B. Bersuker, *The Jahn-Teller effect and vibronic interactions in modern chemistry*, Modern Inorganic Chemistry, Plenum Press, **1983**.

Received: August 20, 2001
Revized: April 16, 2002 [F3499]